EUROFUSION WPPFC-PR(16) 14694

M Balden et al.

Effect of the surface temperature on surface morphology, D retention and erosion of EUROFER exposed to low-energy high-flux D plasma

Preprint of Paper to be submitted for publication in
22nd International Conference on Plasma Surface Interactions
in Controlled Fusion Devices (22nd PSI)

This work has been carried out within the framework of the EUROfusion Consortium and has received funding from the Euratom research and training programme 2014-2018 under grant agreement No 633053. The views and opinions expressed herein do not necessarily reflect those of the European Commission.

Effect of the surface temperature on surface morphology, D retention and erosion of EUROFER exposed to low-energy high-flux D plasma

M. Balden[a], S. Elgeti[a], M. Zibrov[a,b,c,d,e], K. Bystrov[b], T.W. Morgan[b]

[a] *Max-Planck-Institut für Plasmaphysik, Boltzmannstraße 2, D-85748 Garching, Germany*

[b] *FOM Institute DIFFER, De Zaale 20, 5612 AJ Eindhoven, The Netherlands*

[c] *Gent University, Sint-Pietersnieuwstraat 41, B-9000 Gent, Belgium*

[d] *Physik-Department E28, Technische Universität München, James-Franck-Straße 1, D-85748 Garching, Germany*

[e] *National Research Nuclear University MEPhI (Moscow Engineering Physics Institute), Kashirskoe shosse 31, 115409 Moscow, Russia*

Martin.Balden@ipp.mpg.de

Abstract: Samples of EUFROFER, a reduced activation ferritic martensitic steel, were exposed in the Pilot-PSI device to deuterium (D) plasma with incident ion energy of ~40 eV and incident D flux of 2-6×10^{23} D/m^2s up to a fluence of 10^{27} D/m^2 at surface temperatures ranging from 400 K to 950 K. The main focus of the study lays on the surface morphology changes dependent on the surface temperature and the surface composition evolution, e.g., the enrichment in tungsten; but also the erosion and the D retention are studied. The created surface morphology varies strongly with surface temperature from needle-like to corral-like structures. The visible lateral length scale of the formed structures is in the range of tens of nanometres to above 1 µm and exhibits two thermal activated regimes below and above ~770 K with activation energies of 0.2 eV and 1.3 eV, respectively. The enrichment of heavy elements on the surface is correlated to the surface morphology at least in the high temperature regime, independent of the origin of the enrichment (intrinsic from the sample or deposited by the plasma). Also the erosion exhibits a temperature dependence at least above ~770 K as well as a fluence dependence. The deuterium is mainly retained in the top 500 nm. Its amount is almost independent of the exposure temperature and is of the order of 10^{18} D/m^2, which would correspond to a sub-mono layer D coverage on the surface.

Keywords: plasma facing material; surface morphology; erosion; steel; plasma exposure

Highlights:

- Strong temperature effect on surface morphology of EUROFER by D plasma exposure
- Two thermal activation energy (0.2 and 1.3 eV) determined for morphology formation
- Surface structure are decorated with tungsten (enrichment)

1. Introduction

Reduced Activation Ferritic Martensitic (RAFM) steels are the primary choice in future fusion power plants for first wall and breeding blanket structural material. In recent years the use of bare RAFM steel without a protective amour (e.g., tungsten (W)) has been proposed as plasma-facing material (PFM) in recessed areas due to technologic and economic reasons [1]. Therefore, the behaviour of RAFM steels under intensive energetic particle and heat load, especially the erosion and hydrogen retention is under investigation to answer the question whether bare RAFM steels can be used as PFM in the main chamber of DEMO [2-4]. It is expected that the small concentration of W contained in RAFM steels such as EUROFER, RUSFER, CLAM and F82H enriches on the surface due to preferential sputtering and, therefore, mitigates the unacceptable high sputter erosion of Fe [3]. In the frame of this exploration strong surface morphological changes were observed [4-9].

This study focuses on the effect of the sample temperature on the surface morphological changes, but tackles also W enrichment, erosion and D retention. The investigated material EUROFER contains high Z-elements: 1 wt% W and 0.1 wt% Ta [10]. Polished EUROFER samples were exposed to D plasmas in the linear plasma generator Pilot-PSI at sample temperature ranging from 400 K to 950 K. Steady-state exposures with incident ion energy ~40 eV and incident D flux of 2-6×10^{23} D/m^2s were performed up to a fluence of 10^{27} D/m^2.

The temperature evolution and its lateral distribution on each sample during plasma exposure were recorded by an IR camera. Surface morphology was investigated before and after exposure by scanning electron microscopy (SEM) and confocal laser scanning microscopy (CLSM). Erosion was studied by weight loss and by marker technique using focused ion beam (FIB), the W and Ta enrichment by Rutherford backscattering (RBS) and Energy Dispersive X-ray spectroscopy (EDX) and the D retention by nuclear reaction analysis (NRA).

2. Experimental

2.1. Samples and pre-characterisation

From a EUROFER plate [11] 19 samples of 15x12x1.1 mm^3 were cut. They were polished to mirror finish, cleaned in isopropanol and then annealed at 870 K for 2 h to reduce hydrogen content and relieve stresses produced by manufacturing and polishing. No significant structural

modifications in the samples are expected at this temperature as microstructural studies after long-term ageing at 870 K show [12]. Thereafter the centres of the samples were imaged with SEM, marked with FIB for easy re-positioning after plasma exposure and areas of 25 – 100 µm^2 were coated with a Pt-C protection layer of 1 - 4 µm thickness used for erosion studies (Helios Nanolab 600, FEI). Finally, all samples were weighted (Satorius MC21S) with an accuracy of 1 µg by multiple weighing and sealed in evacuated plastic bags to prevent contamination, e.g. oxidation.

In addition, 4 pure iron plates of 15x12x1 mm^3 were used as reference samples (purity 99.5 wt%, Goodfellow). They were mirror-polished, annealed at 800 K for 10 minutes, weighted and sealed in a bag, too.

2.2. Deuterium plasma exposure at Pilot-PSI

The samples were exposed to a pure D plasma in the linear plasma generator Pilot-PSI (DIFFER, The Netherlands) [13]. The base pressure was ~10^{-1} Pa which increased to ~1 Pa during the plasma operation. The D plasma was generated in a DC cascaded arc source and guided by an axial magnetic field of 0.2 T to the target allowing steady-state exposure. The plasma beam consisted mainly of D^+ ions [14]. The impurity content in the plasma beam was not measured in the present experiments.

Thomson scattering ~2 cm in front of the target was used to determine electron density n_e and temperature T_e profiles of the plasma beam [15]. The profiles had approximately Gaussian radial distribution with $n_e < 10^{20}$ m^{-3} and $T_e < 1.1$ eV in the maximum. The ion flux density on the targets was estimated according to the Bohm criterion [16]. The resulting spatial flux distribution had a Gaussian profile with a full width at half maximum (FWHM) of 15-20 mm (Fig. 1). The maximal flux varied in the range of 2-6×10^{23} D/m^{2}s between the different exposures, but fixed for each sample. The adjustment between the different coordinate systems, namely, beam centre (flux measurement), sample centre (analyses positions), and IR-camera is better than ±0.5 mm.

The exposure time for the two aimed fluence in the centre of the sample, 2 and 10×10^{26} D/m^2, was determined by a rough evaluation of the Thomson scattering data while the experiment run. Steady-state exposures times between 7 and 48 minutes were applied. The ramping up and down of bias and magnetic field requires a few seconds introducing a negligible fluence uncertainty. The fluence values obtained by the post-evaluation of the Thomson scattering data vary less than 20% from the aimed one for the centre. Note, by taking the Gaussian flux profile into account, the averaged fluence across the exposed area on the sample is about 15% lower than in the centre. Overall, the aimed total fluence for the sample centre is state throughout the article, even for positions outside the sample centre. Note that for one sample (#13) the total fluence was acquired in 8 pulses, i.e., the plasma was 8 times switched on and off without any deviating behaviour compared to the steady-state exposed samples.

A bias voltage of -40 V was applied to the target holder during all exposures to avoid arcing present at higher bias. The incident ion energy is not exactly known because the plasma potential was not measured during the experiments presented here, but is estimated to be a few eV (<5 eV). Therefore, incident ion energy is slightly below 40 eV.

The temporal evolution of the surface temperature (T_s) across the samples was recorded by a fast infrared (IR) camera (Flir SC7500MB) measuring in the wavelength range of 3.5-5 µm. Temperature values were obtained under the assumption that (i) the IR background level did not change with switching on the bias and the magnetic field, that (ii) the samples had an estimated emissivity of 0.25 before plasma exposure [17], and that (iii) the emissivity did not change in the start-up phase of the plasma and stabilisation phase of the surface temperature (< 30 s). The T_s values given in this paper were taken just after the stabilization phase.

The samples were mounted onto the sample holder of Pilot-PSI with a TZM (molybdenum alloyed with titanium and zirconium) clamping ring with a rectangular hole of ~12×10 mm^2 with rounded edges defining the plasma exposed surface area. The thermal contact to the water-cooled copper base plate of the sample holder was obtained by a flexible graphite foil (Grafoil®). To achieve higher surface temperatures than ~400 K, the physical contact of the sample with the holder was varied, e.g., by cutting a hole into the foil beneath the exposed area. A T_s variation across each sample occurred due to the *interplay of beam heating and cooling by thermal conduction* (Fig. 1). With changing the source current and the gas flow in the plasma source, a fine-tuning of T_s of the sample centre (T_{centre}) was done during the stabilisation phase (<30 s). The final temperature distribution was determined by post-analysis of the IR data, mainly along the central line, on which the most post-characterisations were performed (Fig. 2). Furthermore, the maximum temperature (T_{max}) of each sample after reaching equilibrium was determined beside the temperature of the centre (T_{centre}). Surface temperatures between ~400 and ~950 K were obtained, for which an accuracy not better than ±30 K is assumed.

Table 1 lists the aimed total fluence, the temperature of the sample centre T_{centre}, the maximum temperature T_{max} and its distance from the sample centre for all samples data are presented in the article.

2.3. Post-characterisation

The mass loss was determined by multiple weighing with an accuracy of 1 µg and was used to estimate the average erosion yield. To check the mass change due to handling, one sample was mounted without any exposure leading to mass change below 3 µg. This is negligible compared to the mass loss due the plasma exposure.

The surface morphology was analysed by SEM and CLSM on various positions across the sample (Fig. 2), especially around the Pt-C markers in the centre of the samples. The W enrichment and the presence of impurities was measured by RBS (0.69 and 3.2 MeV ^{3}He)

averaged over the 1 mm^2 large analysis spot and by EDX in SEM with lateral resolution of several tens of nanometres. The erosion depth and the thickness of affected layer were obtained by FIB cross-sectioning through the Pt-C-coatings with following SEM imaging and from stereoscopic evaluation from SEM images taken at different tilt angle.

The D content was determined by NRA using the D(^{3}He,p)α reaction with 690 keV and 3.2 MeV ^{3}He measured simultaneously with the RBS about a month after exposure. The measurements were calibrated by using a thin a-C:D layer with a known D content. On each sample 2-4 RBS/NRA measurements were performed along the central line as marked in Fig. 2 and the individual surface temperature of the analysis point was assigned from T_s profiles (Fig. 1). Such temperature assignment was also done for each SEM image.

3. Results and discussion

3.1. Flux and temperature profile

Fig. 1 shows a typical plasma flux profile as well as four T_s profiles after temperature equilibrium is reached of three different samples. The T_s profiles follow in general the Gaussian flux profiles resulting in a similar width for both profiles (see squares in Fig. 1). But for some samples the maximum of the surface temperature deviates more from the sample centre than the positioning accuracy between the different coordinate systems, e.g., along the central line of sample #07 in Fig. 1. This deviation is presumable caused by an asymmetric thermal contact between sample and holder. Note that for these shifts out of the centre, the highest temperature moves during the equilibrium phase from the centre just after the exposure start to the final position at the end of the stabilisation phase. Due to this off-set between T_{max} and flux, the effect of fluence and flux on the morphology can be separated from that of temperature at least for same samples (e.g. sample #7).

3.2. Morphological changes

In the visual inspection, the hottest areas, i.e., corresponding to the T_s evaluation, are visible as dark (brownish-black) areas due to changes of the optical properties for visible light; see for examples Fig. 2.

In Fig. 3 SEM images of sample #7 exposed to 2×10^{26} D/m^2 are presented which correspond to the positions along the marked central line shown in Fig. 2 with varying T_s between 610 and 930 K. For comparison, a surface image of the centre of this sample before exposure is given (Fig. 3(a)) showing the grain structure and the distribution of the precipitated carbide grains of the bare material [12]. Note Figs. 3(a) and 3(h) showing the same area of the centre of sample #7. To complete the investigated T_s range, the centre of a specimen (#2) with desired good thermal contact, i.e., low surface temperature is shown in Fig. 3(b). Furthermore, the surface of a pure Fe sample after exposure is shown in Fig. 3(c), too.

From the images of the exposed surface of sample #7, it follows clearly that the surface exhibits strong morphological changes by the D exposure dependent on the local surface temperature. “Fence/corral”-like structures composed of a network of ridges are found for temperatures above ~770 K. Their tops are enriched in W (and Ta) as determined by EDX-mapping (see section 3.3). This structure and enrichment is observed on all samples at areas above 770 K. The lateral length scale of the “fence/corral”-like structure increases with increasing temperature. These length scales are not correlated to any length of the microstructure of the base material (Fig. 3(a)). Note that for some samples, no indications are left from the grain structure (Fig. 3(f-i)), while for some other samples the grain structure is highlighted by smooth W enriched bands (not shown). The “fence/corral”-like structure and the enrichment is not explainable by erosion only. Diffusion processes (mobility) are needed to get the morphology changes. As only heating of the samples does not lead to such structure, it could be speculated that the presence or the impact of D promotes this diffusion. On the other hand only deposition of W at elevated temperature (see section 3.3), as valid for the pure Fe sample shown in Fig. 3(c), may play the major role in the morphology formation. It is remarkable that the pure Fe samples exhibit the same morphology as the EUROFER (compare Figs. 3(c) and 3(f)).

For lower temperatures, below ~770 K, the original grain structure is always preserved (Fig. 3(b,d,e)). A roughness on the length scale of tens of nanometres is present (Fig. 3(d,e)) which reduces with decreasing temperature and gets too tiny to be measured for temperatures below ~570 K. Furthermore, the carbide grains along the grain boundaries are protruding from the plasma exposed surface (Fig. 3(d,e)). This is the opposite for the lowest temperatures, e.g. 410 K in Fig. 3(b): For such low temperatures it is multiple confirmed by analysing the same area before and after plasma exposure that carbide grains visible on the polished surface before exposure are removed leaving holes, while the areas in between appear smooth.

The nanometre scaled structures are shown in Fig. 4(a) at higher magnification and under a viewing angle to the surface normal of 52°. It is more a needle-like structure. Note that the appearance of surface structures under a viewing angle could be strongly altered. The estimated height of these structures is of the order of 100 nm (Fig. 4(a)), definitely smaller than for the “fence/corral”-like structures at higher temperatures with height of a few 100 nanometres (Fig. 4(b), see also section 3.4).

The samples exposed to high fluence (10^{27} D/m^2) exhibit the same evolution of the surface modifications with temperature. Their five times higher fluence does not lead to different morphology.

To elucidate the mechanism for the “fence/corral”-like and the nanometre scaled structures, their lateral periodicity was determined, e.g., by counting the crossings of a line of distinct length by the features for many lines in the SEM images. Fig. 5 summaries the obtained lateral periodicity for several areas with temperature between 580 and 930 K in an Arrhenius-type plot showing a quite good agreement of data from different sample. Clearly, two distinct thermal

activated processes take action in the formation of observed morphologies. The kink at ~770 K coincides with the change from needles (below 770 K) to “fence/corral”-like structures (above 770 K). The obtained activation energies are 0.2 and 1.3 eV, respectively, and no definite processes could be assigned to these energies up to now. Possible processes are radiation-induced surface segregation (RIS) [18], radiation-enhanced diffusion (RED) [18] or hydrogen-enhanced surface diffusion.

3.3. Enrichment of tungsten, tantalum and molybdenum

The amount of W, Ta and Mo on the surface is quantified from RBS spectra. Fig. 6(a) shows some raw RBS spectra with the signal for W+Ta on the surface in the channels 630-650 and from the bulk below the channel 630, for Mo on the surface in the channels 600-610 and for Fe (and Cr) below channels 550. Note contributions from W and Ta could not be separated. The signals for W+Ta and Mo on the surface are converted into areal densities, ending up with densities in the order of 10^{19} at/m^2, i.e., several monolayers. Fig. 6(b) shows the W+Ta areal density in addition the one of unexposed surface versus the temperature of the individual analysis spots. The analogous graph for Mo looks similar to Fig. 6(b) but with overall lower areal densities, which are below the detection limit at several analysing spot. It is remarkable that the agreement of data for the same temperature from different sample is quite good.

Obviously, some W+Ta and Mo arrive together with plasma beam, as indicated by the amount of W+Ta on the pure Fe samples (Fig. 6(b)). As the data points of pure Fe fall onto those from EUROFER, clearly the enrichment is dominated by the W+Ta flux from the plasma compared than W+Ta coming from the EUROFER itself. Furthermore, the amount of W+Ta clearly increases with temperature. The variation of flux could be excluded, i.e., for sample #7 areas with the same distance from the sample centre had different temperatures, e.g., 760 K and 930 K. The reason for the temperature dependence is unclear. An effect of the morphology on the RBS signal needs further evaluation.

Fig. 7 shows an example for the lateral distribution of the W+Ta and Fe. These distributions clearly follow the structures presented in Fig. 3 indicating diffusion processes of the arriving and intrinsic W+Ta. Note that, in order to restrict the interaction volume of the electron beam within the nanostructure and increase the sensitivity for the surface layer, a low primary energy for the electron beam was used. Therefore, only the low energy characteristic X-ray of W and Ta are excite, for which the energy resolution of EDX detector is not sufficient to separate them, if Ta amount is significantly smaller than W amount. Nevertheless, at some location definitely Ta was observed. Therefore, only amounts of sum of W+Ta are given in the article. Furthermore, from the EDX mapping it could be concluded that a small amount of Mo is present and its lateral distribution follows that of W+Ta.

3.4. Erosion

The mass loss value for each individual sample is only a measure of the averaged erosion over different T_s, fluxes and fluences distributed across the sample during loading (section 3.1). The mass loss values of all samples assigned to the maximal temperature T_{max} of each sample are presented in Fig. 8. Increasing erosion with increasing temperature is obvious. From the data it could not be decided if this increase starts only above ~770 K or extent over the full investigated temperature range, i.e. if only one of the thermal activated processes leads to a temperature dependent erosion (see section 3.2).

Remarkable, the value for the 10^{27} D/m^2 fluence are only a factor of 2-3 higher than the value for the 2×10^{26} D/m^2 fluence, i.e., the erosion yield decreases with fluence, pointing to a fluence dependence of the erosion yield due to the enrichment of W+Ta.

Assuming homogenous erosion across the exposed area, i.e., ignoring the temperature, plasma potential and flux variation across the exposed area, the mass losses can be converted into erosion yields (right axis Fig. 8): Erosion yields are of the order 10^{-5}, which fits reasonable to published data for pure Fe and steels [19, 20], and no impurity fraction in the plasma beam is needed to explain the erosion. The used ion energy is quite close to the threshold of sputtering but, unfortunately, not exactly known.

The thickness of the affected layer is geometrically measured in images of cross-sectioned marker coatings. Two examples are presented in Fig. 9. The surface of EUROFER sample as well as the Pt-C coating show the nanometre scaled structure (Fig. 9(a) and section 3.2). Note that the surface is coated a second time with protection layer for improving the quality of FIB cross sectioning process and that, for the sample #15, the roughness of the surface and the first coating are so high that artefacts of the FIB preparation (curtain effect) dominate the quality of the cross section. But clearly in both cross sections (Fig. 9(b)), the surface below the marker coating is smooth and unaffected while aside the marker it is rough. From the cross section, the thickness of the affected layer by the morphological changes can be determined from the smooth, unaffected surface to the bottom of the roughness with an accuracy of 30 nm. For the two examples in Fig. 9 exposed to the high fluence (10^{27} D/m^2), this thickness is ~170 nm and 390 nm. In the case of sample #15 (Fig. 9(c)) even an overall erosion of ~150 nm is observed. Obtained values for the thickness of the affected layer, i.e., the height of the needles and the ridges by stereoscopic analysis and by 3D profilometry with CLSM, are similar but with a larger uncertainty than from the cross-sectioned markers.

An averaged erosion depth could be calculated from the mass loss assuming homogeneous erosion across the exposed sample surface (~1.5 nm/µg for Fe). The resulting depths are between half and close to equal to the thickness of the affect layer. Therefore, unfortunately it cannot be confirmed or disproved whether the observed structures are purely erosion morphology or grown structures as the tungsten fuzz by helium impact [21, 22].

Note that a W+Ta coverage of 6×10^{19} at/m^2 on the exposed sample area equals to that the amount of W+Ta in a layer of 2.2 µm of EUROFER which is much larger than the eroded layer. Furthermore, this coverage coming from plasma would contribute to sample mass by only ~2 µg, i.e., can be neglected compared to the measured mass loss due to plasma exposure.

3.5. Deuterium retention

The retained D was determined as integral values for the surface layer of <500 nm and for larger depth (< 6 µm). The results for the surface layer for individual points versus their respective T_s are presented in Fig. 10. Nearly all data points are between 1 and 3×10^{18} D/m^2 indicating an independence from T_s and that all D is retained close to the surface. Only the data for the sample with the lowest T_s at about 400 K indicates a higher D retention. And only for this a significant higher D retention beyond the top surface layer is found by NRA with 3.2 MeV ^{3}He (Fig. 10). The higher fluence does not increase the D retention. Interestingly, the pure Fe sample, which forms the same morphology as the EUROFER samples (Figs. 3(c) and 3(c)), exhibits a significant lower D retention.

Overall, the small amount of below 10^{19} D/m^2 could already be explained by a sub-mono layer D coverage on the surface. Which fraction of retained D is absorbed into the material could not be determined from the performed NRA measurements. Measurements of the D retention in volume of the samples by thermal desorption spectrometry are still pending.

4. Conclusion and summary

EUROFER samples were exposed to Pilot-PSI plasma up to fluences of 10^{27} D/m^2 with an ion energy of ~40 eV. The surface morphology created by the exposure varies strongly with the surface temperature in the investigated temperature range from 400 K to 950 K.

The length scale, i.e., lateral periodicity of the surface structure obeys Arrhenius behaviour with two activation energies (1.3 eV, 0.2 eV). Above ~770 K, the higher activation energy determines the structure formation leading to “fence/corral”-like structure composed of a network of ridges. The tops of the ridges are enriched in tungsten (and tantalum). For temperatures below ~770 K, the surface morphology is composed of needles. Their tips seem to be covered with W+Ta, too. This lateral distribution of W+Ta, which is not correlated to its distribution in EUROFER or is not homogenously, indicates mobility for W (and Ta).

The amount of W comes only partially from the EUROFER itself by preferential sputtering and diffusion, but the main fraction arriving with the plasma. Therefore, the possible enhanced segregation of W and Ta out of Fe in the presence of hydrogen (even above the solubility limit) cannot be confirmed or ruled out. It has to be stated that the ratio of observed W+Ta amount to the D fluence is of the order of 10^{-7}. Such low fraction of impurity is experimentally very hard accessible and should be kept in mind for the interpretation of other not mass-separated

exposures and the comparison of the results obtained from them. On the other hand, in fusion devices with steel and tungsten as PFM, it could be expected that some tungsten will arrive together with the hydrogen and helium on the plasma-facing areas proposed for steel. This could then lead to morphology as shown in Fig. 3.

Overall, the thermal activated formation of the surface morphology affects the erosion of RAFM steel. Fluences needed to achieve steady state erosion will be many orders of magnitude higher compared to those obtained from simple TRIM simulations [23, 24] and even in more advanced simulations [25]. Therefore, the predicted reduction of erosion of the RAFM steel by W enrichment will be lower. Nevertheless, a reduction of the erosion with fluence, i.e., with W enrichment was observable in our and other studies [3, 24, 26].

The deuterium retention in the first micrometres under our condition is quite low, only of the order of 10^{18} to 10^{19} D/m^2 and roughly independent of temperature. This small amount would correspond to sub-monolayer of coverage of deuterium on the surface. In the literature quite contradicting values and temperature dependencies of D retention in RAFM steels are given [4, 6, 26-28] pointing to complex interplay of many parameters.

Acknowledgments

This work has been carried out within the framework of the EUROfusion Consortium and has received funding from the Euratom research and training programme 2014-2018 under grant agreement No 633053. The views and opinions expressed herein do not necessarily reflect those of the European Commission. Work was performed under EUROfusion WP PFC. Furthermore, this project was carried out with financial support from NWO. Finally, thanks to T. Schwarz-Selinger, K. Sugiyama, H. Maier, U. von Toussaint, G. Matern, T. Höschen, M. Fußeder and J. Dorner for sample preparation, technical assistance, and fruitful discussions.

References

[1] H. Bolt *et al.*, J. Nucl. Mater. 307–311 (2002) 43

[2] K. Tsuzuki *et al.*, Nuclear Fusion 46 (2006) 966

[3] J. Roth *et al.*, J. Nucl. Mater. 454 (2014) 1

[4] V.Kh. Alimov *et al.*, Phys. Scripta T159 (2014) 014049

[5] V.Kh. Alimov *et al.*, Nucl. Mater. & Energy xxx (2016) xxx, doi:10.1016/j.nme.2016.01.001

[6] N. Ashikawa, K. Sugiyama, A. Manhard, M. Balden and W. Jacob, "Effects of surface modifications on deuterium retention in F82H and EUROFER exposed to low-energy deuterium plasmas", accepted for publication in Fusion Engineering and Design, http://dx.doi.org/10.1016/j.fusengdes.2016.04.029

[7] M. Raciniski *et al.*, Phys. Scr. T167 (2016) 014013

[8] W. Jacob *et al.*, "RAFM Steels as an Option for a Plasma-Facing Material at the First Wall of Demo", I22 and M. Racinski *et al.*, "Surface Morphology and Composition of Eurofer Steel and Fe-W Model Alloys after Deuterium Plasma Exposure", O91, ICFRM-17, Oct. 2015, Aachen, Germany

[9] M. Balden *et al.*, "Surface modifications of RAFM steels by D exposure: Variation from coral-like/fuzz-like to blister-like features", P3-20, PSI-21, May 2014, Kanazawa, Japan

[10] R. Lindau *et al.*, Fusion Engineering and Design 75-79 (2005) 989-96

[11] EUROFER reference number (plate no 93/A1/2, cast 993 393)

[12] P. Fernandez *et al.*, J. Nucl. Mater. 307-11 (2002) 495-9[13] G.J. van Rooij, V.P. Veremiyenko, W.J. Goedheer, B. de Groot, A.W. Kleyn, P.H.M. Smeets, T.W. Versloot, D.G. Whyte, R. Engeln, D.C. Schram, N.J.L. Cardozo, Applied Physics Letters, 90 (2007) 121501.

[14] R.C. Wieggers, P.W.C. Groen, H.J. de Blank, W.J. Goedheer, Contributions to Plasma Physics, 52 (2012) 440-444.

[15] H.J. van der Meiden, R.S. Al, C.J. Barth, A.J.H. Donné, R. Engeln, W.J. Goedheer, B. de Groot, A.W. Kleyn, W.R. Koppers, N.J. Lopes Cardozo, M.J. van de Pol, P.R. Prins, D.C. Schram, A.E. Shumack, P.H.M. Smeets, W.A.J. Vijvers, J. Westerhout, G.M. Wright, G.J. van Rooij, Review of Scientific Instruments, 79 (2008) 013505.

[16] P.C. Stangeby, "The Plasma Boundary of Magnetic Fusion Devices", IOP Publishing Ltd., Bristol and Philadelphia, 2000.

[17] M. Kobayashi, A. Ono, M. Otsuki, H. Sakate, F. Sakuma, International Journal of Thermophysics 20 (1999) 299-308

[18] G. Was, Progress in Surface Science, 32 (1990) 211

[19] W. Eckstein, C. García-Rosales, J. Roth, W. Ottenberger, "Sputtering Data", IPP Report 9/82 (1993), Max-Planck-Institut für Plasmaphysik, Garching, (http://hdl.handle.net/11858/00-001M-0000-0027-6324-6)

[20] K. Sugiyama, K. Schmid, W. Jacob, Nucl. Mater. & Energy 8 (2016) 1-7

[21] S. Kajita *et al*., J. Nucl. Mater. 418 (2011) 152-8

[22] S. Kajita *et al*., Nuclear Fusion 49 (2009) 095995

[23] U. von Toussaint, Mutzke A., Sugiyama K, and Schwarz-Selinger T., Phys. Scr. T167 (2016) 014023

[24] K. Sugiyama *et al*., J. Nucl. Mater. 463 (2015) 272-5

[25] U. von Toussaint, A. Mutzke, "Erosion and Surface Morphology study of iron-tungsten model system towards assessment of reduced activation ferritic martensitic steel (EUROFER) as plasma-facing material", P1.5, PSI-22, May 2016, Rome, Italy

[26] O. V. Ogorodnikova, Z. Zhou, K. Sugiyama, M. Balden, Yu. Gasparyan, V. Efimov, "Surface modification and deuterium retention in reduced-activation ODS steels under the low-energy deuterium plasma exposure Part I: undamaged steels", submitted to Nuclear Fusion

[27] A.V. Golubeva *et al*., J. Nucl. Mater. 438 (2013) S983–S987

[28] Y. Hatano *et al*., Fusion Eng. Des. 67 (2015) 361

Sample id	Fluence [10^{26} D/m^2]	T_{centre} [K]	T_{max} [K]	Distance [mm]
#02	2	410	410	0
#04	2	580	580	0
#05	2	770	780	1
#06	2	820	840	1
#07	2	910	940	1
#08	2	480	480	0
#09	2	630	640	1
#10	2	760	770	1
#11	2	950	960	0.5
#12	10	820	830	0.5
#13	2 pulsed	760	760	0
#14	2	820	830	1
#15	10	820	840	2
#16	10	730	750	1
#18	2	800	930	4
#19	2	770	830	1
Fe#1	2	380	380	0
Fe#2	2	>550	>750	2
Fe#3	10	390	390	0
Fe#4	2	780	790	1

Tab. 1: Aimed total fluence, temperature of the sample centre T_{centre}, the maximum temperature T_{max} and its distance from the sample centre for the exposed EUROFER samples (#2-#19) and pure iron samples (Fe#1-4).

Figures

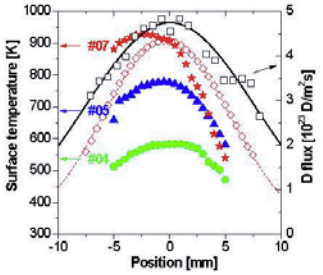

Fig. 1: Temperature profiles across the central line of three samples (filled symbols) and along the sample diagonal for sample #7 (open diamonds) and a typical radial distribution of incident ion flux (open squares). Zero position corresponds for all samples to the samples centre, i.e., beam centre. Note, for some samples the maximum of the surface temperature deviates from the samples centre. The temperature profiles were taken just after the plasma start-up and temperature stabilisation. The solid and dashed lines are Gaussian fits with a FWHM of 16.9 and 13.5 mm for the flux and the temperature profile (300 K baseline), respectively.

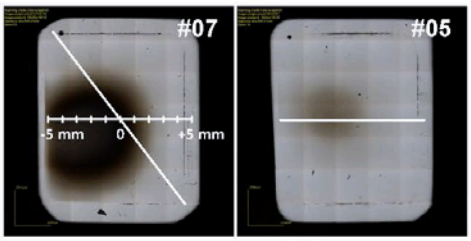

Fig. 2: Stitched optical microscope images of two samples after plasma exposure (2×10^{26} D/m^2; ~40 eV). The central horizontal lines, on which NRA/RBS analyses and mainly SEM are made, as well as one diagonal are marked. Along these lines the T_s profiles are obtained and given in Fig. 1.

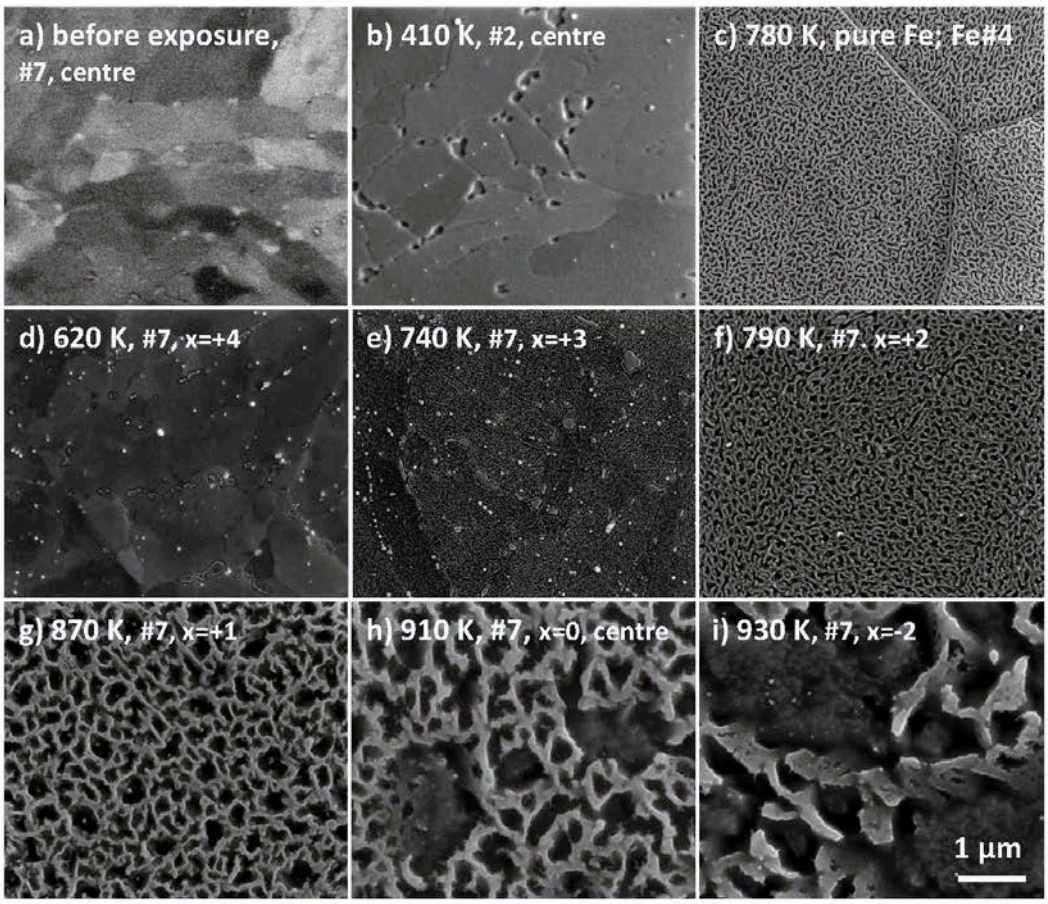

Fig. 3: SEM images: (a) of the centre of EUROFER sample #7 before exposure, (b) of the centre of EUROFER sample #2 after exposure, (c) of the centre of a pure Fe sample (Fe#4) after exposure, and (d-i) of sample #7 after exposure along the central line at 6 positions (see Fig. 2) with the distance from centre given in millimetre. The individual surface temperature of each analysis position is indicated in the images. All samples were exposed to 2×10^{26} D/m^2 and ~40 eV. All SEM images are taken with the same magnification and the electron beam perpendicular to the surface.

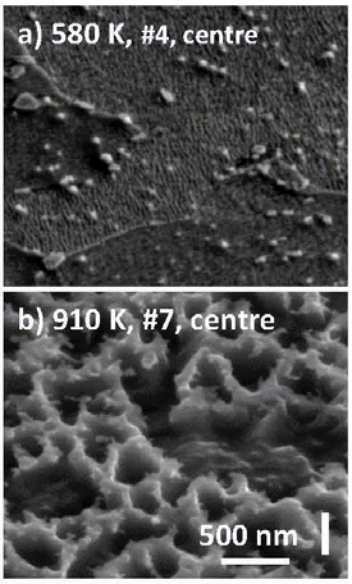

Fig. 4: SEM images (a) of centre of EUROFER sample #4 after exposure at ~580 K and (b) of sample #7 at ~910 K (2×10^{26} D/m^2; ~40 eV). The SEM images are taken with the same magnification and after tilting by 52° in respect to the electron beam around the x-axis. Note (b) shows the central area of Fig. 3(h) in higher magnification.

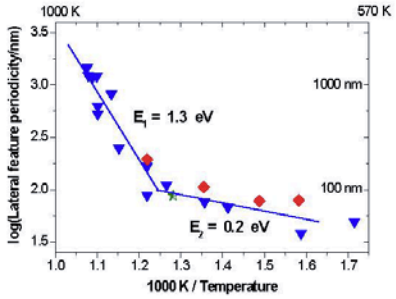

Fig. 5: Arrhenius-plot of the lateral periodicity of the structure of exposed surface of various EUROFER samples (triangles: 2×10^{26} D/m^2; diamonds: 10^{27} D/m^2) and of a pure Fe sample (Fe#4, star: 2×10^{26} D/m^2) as obtained from SEM images.

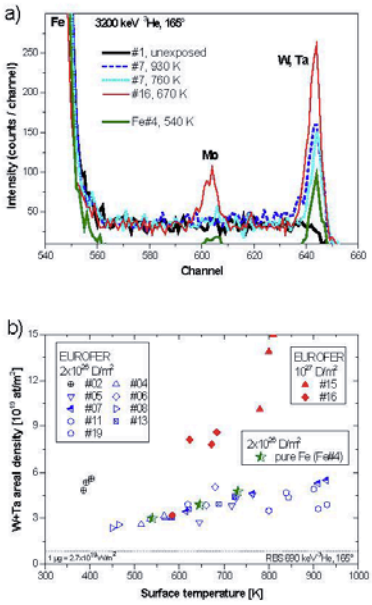

Fig. 6: (a) Example RBS spectra of 3.2 MeV ^{3}He measured for different samples and discharge showing peaks of the W/Ta, Mo and Fe on the surface; (b) the areal density of W+Ta versus T_s for many samples (open symbols: 2×10^{26} D/m^2; filled symbols: 10^{27} D/m^2) obtained from RBS spectra of 690 keV ^{3}He.

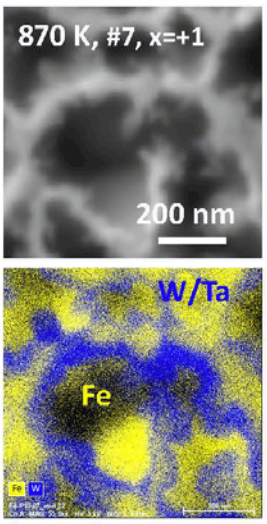

Fig. 7: (a) SEM image in SE contrast close to the centre (+1 mm) of samples #7 (2×10^{26} D/m^2; ~40 eV); (b) same area as composed EDX elemental map for Fe (yellow) and W+Ta (blue). The bright structures in (a) are obviously enriched in W+Ta (b). Note, the energy resolution of EDX detector under used conditions is not sufficient to separate W and Ta and the Fe signal is shadowed from the ridges.

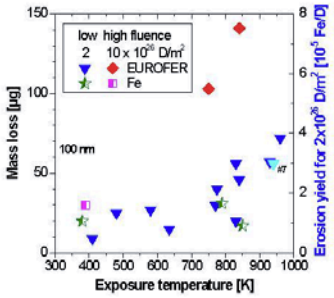

Fig. 8: Mass loss of all samples versus their maximal temperature. The right axis is only valid for a fluence of 2×10^{26} D/m^2 onto the exposed area (~1.2 mm^2). The thickness of the averaged eroded layer is indicated (1.5 nm/µg).

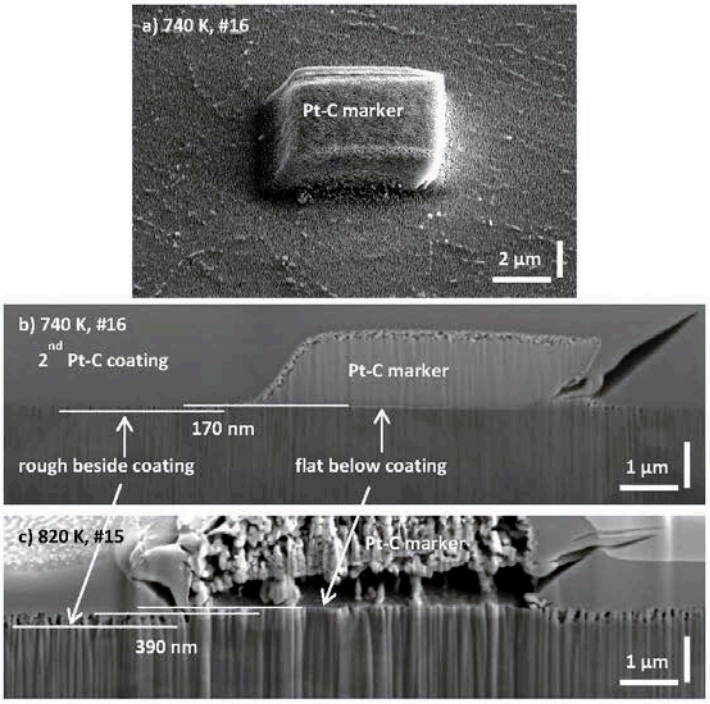

Fig. 9: SEM images (a) of the exposed surface of sample #16 (1×10^{27} D/m^2; ~40 eV) with the Pt-C marker (viewing angle 52°), (b) of the same marker after FIB cross-sectioning (viewing angle -38°) and (c) of the cross-section through a Pt-C marker after exposure (1×10^{27} D/m^2; ~40 eV) of sample #15 (viewing angle -38°). The surface temperature of these areas during the exposure is indicated. The layer thickness of the surface structure due to the exposure (from level of flat surface below coating to bottom of the changes structure) is measured and given in the figure. A second protection Pt-C coating onto the Pt-C marker and the exposed surface was made before FIB cross-sectioning

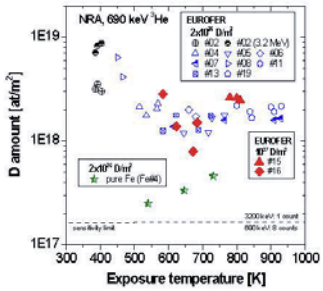

Fig. 10: Deuterium retention of all analysed samples exposed to 2 (open symbols) and 10×10^{26} D/m^2 (larger, complete filled symbols) versus the surface temperature at the individual analysis spot by NRA with 690 keV ^{3}He (<500 nm). Only for sample #2 (lowest temperature) also the NRA data obtained with 3.2 MeV ^{3}He (<6 µm) are given because only for that sample they differ significantly from those for the top 500 nm.